

# Effects of Process Parameters on Deformation and Temperature Uniformity of Forged Ti-6Al-4V Turbine Blade

Shiyuan Luo, Dahu Zhu, Lin Hua, Dongsheng Qian, Sijie Yan, and Fengping Yu

(Submitted January 21, 2016; in revised form August 21, 2016; published online September 9, 2016)

This work is motivated by the frequent occurrence of macro- and microdefects within forged Ti-6Al-4V turbine blades due to the severely nonuniform strain and temperature distributions. To overcome the problem of nonuniformity during the blade forging operation, firstly, a 2D coupled thermo-mechanical finite element approach using the strain-compensated Arrhenius-type constitutive model is employed to simulate the real movements and processing conditions, and its reliability is verified experimentally. Secondly, two evaluation indexes, standard deviation of equivalent plastic strain and standard deviation of temperature, are proposed to evaluate the uniformity characteristics within the forged blade, and the effects of four process parameters including the forging velocity, friction factor, initial workpiece temperature and dwell time on the uniformity of strain and temperature distributions are carefully studied. Finally, the numerically optimized combination of process parameters is validated by the application in a practical process. The parametric study reveals that a reasonable combination of process parameters considering the flow resistance, flow localization and the effects of deformation and friction heating is crucial for the titanium alloy blade forging with uniformity. This work can provide a significant guidance for the design and optimization of blade forging processes.

**Keywords** forging, modeling and simulation, process parameters, turbine blade, uniformity characteristics

## 1. Introduction

Turbine blades are one of the most important mechanical components widely employed in aircraft engines since they play an important role in energy transformation (Ref 1). Due to the complexity of the shape and low formability limits of the material, severely nonuniform strain and temperature distributions are prone to occur in hot forging of the titanium alloy blade, which will not only result in poor forming quality like

**Shiyuan Luo** and **Dongsheng Qian**, School of Materials Science and Engineering, Wuhan University of Technology, Wuhan 430070, China, and Hubei Key Laboratory of Advanced Technology for Automotive Components, Wuhan University of Technology, Wuhan 430070, China; **Dahu Zhu**, Hubei Key Laboratory of Advanced Technology for Automotive Components, Wuhan University of Technology, Wuhan 430070, China, Hubei Collaborative Innovation Center for Automotive Components Technology, Wuhan University of Technology, Wuhan 430070, China, and Blade Intelligent Manufacturing Division, HUST-Wuxi Research Institute, Wuxi 214174, China; **Lin Hua**, Hubei Key Laboratory of Advanced Technology for Automotive Components, Wuhan University of Technology, Wuhan 430070, China, and Hubei Collaborative Innovation Center for Automotive Components Technology, Wuhan University of Technology, Wuhan 430070, China; **Sijie Yan**, Blade Intelligent Manufacturing Division, HUST-Wuxi Research Institute, Wuxi 214174, China, and State Key Laboratory of Digital Manufacturing Equipment and Technology, Huazhong University of Science and Technology, Wuhan 430074, China; and **Fengping Yu**, Technology Center, Wuxi Turbine Blade Co., Ltd., Wuxi 214174, China. Contact email: dhzhu@whut.edu.cn.

## Nomenclature

$A$	Material constant of Arrhenius-type constitutive model
$C$	Heat capacity
$D$	Diameter of preform blade
$E$	Young's modulus
$h$	Convection coefficient to environment
$k$	Shear yield stress
$K_a$	Thermal conductivity
$K_h$	Heat transfer coefficient between workpiece and die
$m$	Friction factor
$n$	Material constant of Arrhenius-type constitutive model
$n'$	Material constant of Arrhenius-type constitutive model
$N_r$	Ratio of forged blade cross-section area to flash cross-section area
$Q$	Activation energy of hot deformation
$R$	Universal gas constant
$S_a$	Cross-section area of final forging blade without flash
$S_e$	Cross-section area of flash
$S_d$	Forging stroke of upper die
$T$	Temperature
$T_d$	Initial temperature of die
$T_e$	Temperature of environment
$T_w$	Initial temperature of workpiece
$v$	Forging velocity
$Z$	Modified Zener-Hollomon parameter

## Greek Symbols

$\alpha$	Material constant of Arrhenius-type constitutive model
$\alpha_t$	Thermal expansion coefficient
$\beta$	Material constant of Arrhenius-type constitutive model
$\rho$	Density
$\tau$	Friction stress
$\sigma$	Flow stress

### Greek Symbols

$\mu$	Poisson's ratio
$\eta$	Emissivity

### Abbreviations

DT	Dwell time before forging
SDP	Standard deviation of equivalent plastic strain
SDT	Standard deviation of temperature

excessively nonuniform microstructure (Ref 2), additional tensile stress (Ref 3), but also cause some macro- and microdefects such as shear bands (Ref 4), void formation (Ref 5) and triple-point cracking (Ref 6) that eventually lead to gross failure (Ref 7). In addition, the deformation and temperature distributions are found to be sensitive to forging conditions, especially the forging velocity (Ref 8), initial workpiece temperature (Ref 9), frictional condition (Ref 10) and dwell time (Ref 11). Hence, to analyze the issue of uniform deformation and temperature is of great importance for process optimization and precise control of part performance.

Until now, a large amount of work has been done in blade forging processes. Focusing on the blade formability, Kang et al. (Ref 12) optimized the slope angle of the die parting line and position of the preform within the die by forward loading and backward tracing simulations to satisfy the final design condition of the blade flashless forging. Ou et al. (Ref 13) investigated material flow, forging force history and die stress of different preform shapes by finite element (FE) simulation. Zhan et al. (Ref 14) investigated the influences of shape and location of the preform on improving the die filling through a 3D FEM approach. Ou et al. (Ref 15) and Lu et al. (Ref 16) employed the FEM to optimize the die profiles for the net-shape forging of aerofoil blade considering the error compensations of forging dies. Kocanda et al. (Ref 17) and Luo et al. (Ref 18) employed a 3D FVM to study the effects of die cavity positioning and frictional condition on lateral forces during the turbine blade forging process, respectively. For the analysis of part performance, Hu et al. (Ref 19) predicted the strain patterns of blade sections using either 2D or 3D analysis and proposed that the 2D analysis is more efficient in a local region. But their work lacked a comprehensive analysis of the influence of forming parameters. In fact, the issue of nonuniform deformation and temperature, as a key evaluation index of the part performance, has received extensive concern. Recent research conducted by Alimirzaloo et al. (Ref 20), Shao et al. (Ref 21) and Torabi et al. (Ref 22) employed the 3D FEM to minimize the strain nonuniformity of the blade by optimizing the preform shape. Their work, however, ignored the effects of forming parameters. Moreover, the application of 3D FEM was largely limited in accurate prediction of the inside nonuniform deformation and temperature of the blade due to the poor quality of interior meshes.

It is observed that, although previous studies have been performed from the aspects of blade formability and part performance to investigate the forming mechanisms using the numerical simulation, none of them is directly tied to the comprehensive analysis of the effects of forming parameters, especially on the inside deformation and temperature uniformity. The benefit of this consideration is that the inside deformation and temperature uniformity can be directly related

to the forming quality. Therefore, the purpose of this paper is to assess the influence of process parameters on the titanium alloy blade forging process. Specifically, the effects of forging velocity, friction factor, initial workpiece temperature and dwell time on inside deformation and temperature uniformity are investigated based on the 2D coupled thermo-mechanical finite element simulations and experimental works.

## 2. FE Modeling and Model Validation

### 2.1 Constitutive Model

A strain-compensated Arrhenius-type constitutive model is employed to predict the rheological behavior of Ti-6Al-4V alloy at elevated temperature which can be expressed as follows (Ref 23):

$$\sigma = \frac{1}{\alpha} \ln \left\{ \left( \frac{Z}{A} \right)^{1/n} + \left[ \left( \frac{Z}{A} \right)^{2/n} + 1 \right]^{1/2} \right\} \quad (\text{Eq 1})$$

$$Z = \dot{\varepsilon} \exp \left[ \frac{Q}{R(T + 273.15)} \right] \quad (\text{Eq 2})$$

$$\dot{\varepsilon} = AF(\sigma) \exp \left[ - \left( \frac{Q}{R(T + 273.15)} \right) \right] \quad (\text{Eq 3})$$

$$F(\sigma) = \begin{cases} \sigma^{n'} & \alpha\sigma < 0.8 \\ \exp(\beta\sigma) & \alpha\sigma > 1.2 \\ [\sinh(\alpha\sigma)]^n & \text{for all } \sigma \end{cases} \quad (\text{Eq 4})$$

$$\alpha = \frac{\beta}{n'} \quad (\text{Eq 5})$$

where  $\sigma$  is the flow stress of the material,  $Z$  is the modified Zener-Hollomon parameter,  $R$  is the universal gas constant,  $\dot{\varepsilon}$  is the strain rate,  $Q$  is the activation energy of hot deformation, and  $A$ ,  $n'$ ,  $\beta$ ,  $\alpha$  and  $n$  are the material constants.

Moreover, in Eq 6, 7, 8, and 9, a fifth-order polynomial is used to represent the influence of strain on material constants. The values of  $n'$  and  $\beta$  and the polynomial fit results of  $\alpha$ ,  $n$ ,  $Q$  and  $\ln A$  of Ti-6Al-4V alloys are obtained from the work of Cai et al. (Ref 24).

$$\alpha = C_0 + C_1\varepsilon + C_2\varepsilon^2 + C_3\varepsilon^3 + C_4\varepsilon^4 + C_5\varepsilon^5 \quad (\text{Eq 6})$$

$$n = D_0 + D_1\varepsilon + D_2\varepsilon^2 + D_3\varepsilon^3 + D_4\varepsilon^4 + D_5\varepsilon^5 \quad (\text{Eq 7})$$

$$Q = E_0 + E_1\varepsilon + E_2\varepsilon^2 + E_3\varepsilon^3 + E_4\varepsilon^4 + E_5\varepsilon^5 \quad (\text{Eq 8})$$

$$\ln A = F_0 + F_1\varepsilon + F_2\varepsilon^2 + F_3\varepsilon^3 + F_4\varepsilon^4 + F_5\varepsilon^5 \quad (\text{Eq 9})$$

### 2.2 Modeling Process

Figure 1(a) presents a 3D schematic diagram of the titanium alloy turbine blade forging operation, from where a complex cross section of the blade body is selected for establishing a 2D coupled thermo-mechanical FE model based on the commercial software Simufact. Forging, as shown in Fig. 1(b). The blade material with a length of 1220 mm used in the model is Ti-6Al-4V. A type of circular preform shape for forging the blade section is adopted, and its diameter can be designed by the following formula (Ref 25):

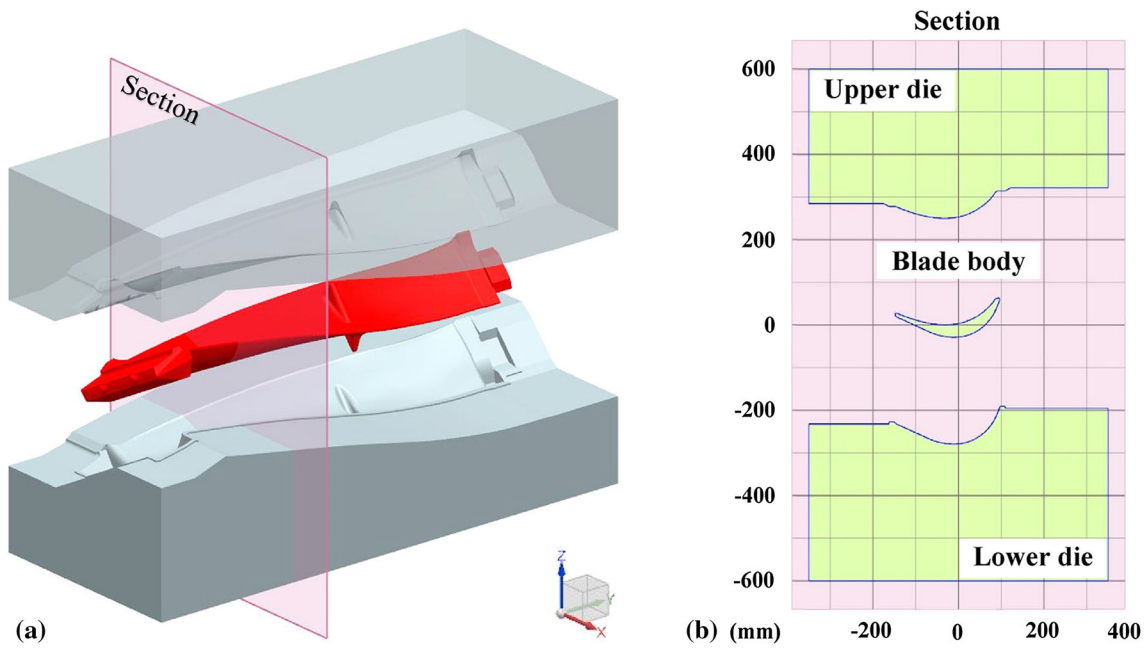


**Fig. 1** 3D geometry model of Ti-6Al-4V turbine blade forging (a) and the blade section selected for establishing 2D FE model (b)

**Table 1** Chemical composition of Ti-6Al-4V alloy (mass fraction, %)

Al	V	Fe	C	H	O	Ti
6.02	3.78	0.08	0.007	0.0082	0.074	Bal.

**Table 2** Important parameters for FE model

$v$ (mm/s)	$S_d$ (mm)	$m$	DT (s)	$T_d$ (°C)	$T_w$ (°C)	$T_e$ (°C)
500 (Ref 20)	59.6	0.4 (Ref 28)	0	250 (Ref 7)	950 (Ref 20)	20
$\mu$	$\rho$ (kg/mm <sup>3</sup> )	$K_h$ [N/(s mm <sup>2</sup> °C)]	$h$ [N/(s mm <sup>2</sup> °C)]	$\alpha_t$ (1/°C)	$\eta$	...
0.342	$4.43 \times 10^{-6}$	5 (Ref 20)	0.02 (Ref 29)	$1.05 \times 10^{-5}$ (Ref 29)	0.7 (Ref 20)	...

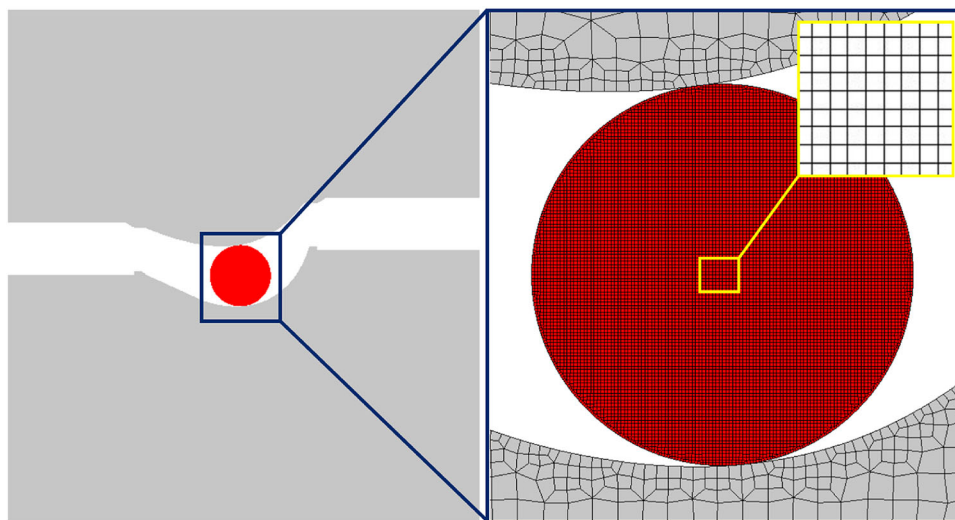


**Fig. 2** Initial position and element type of the workpiece

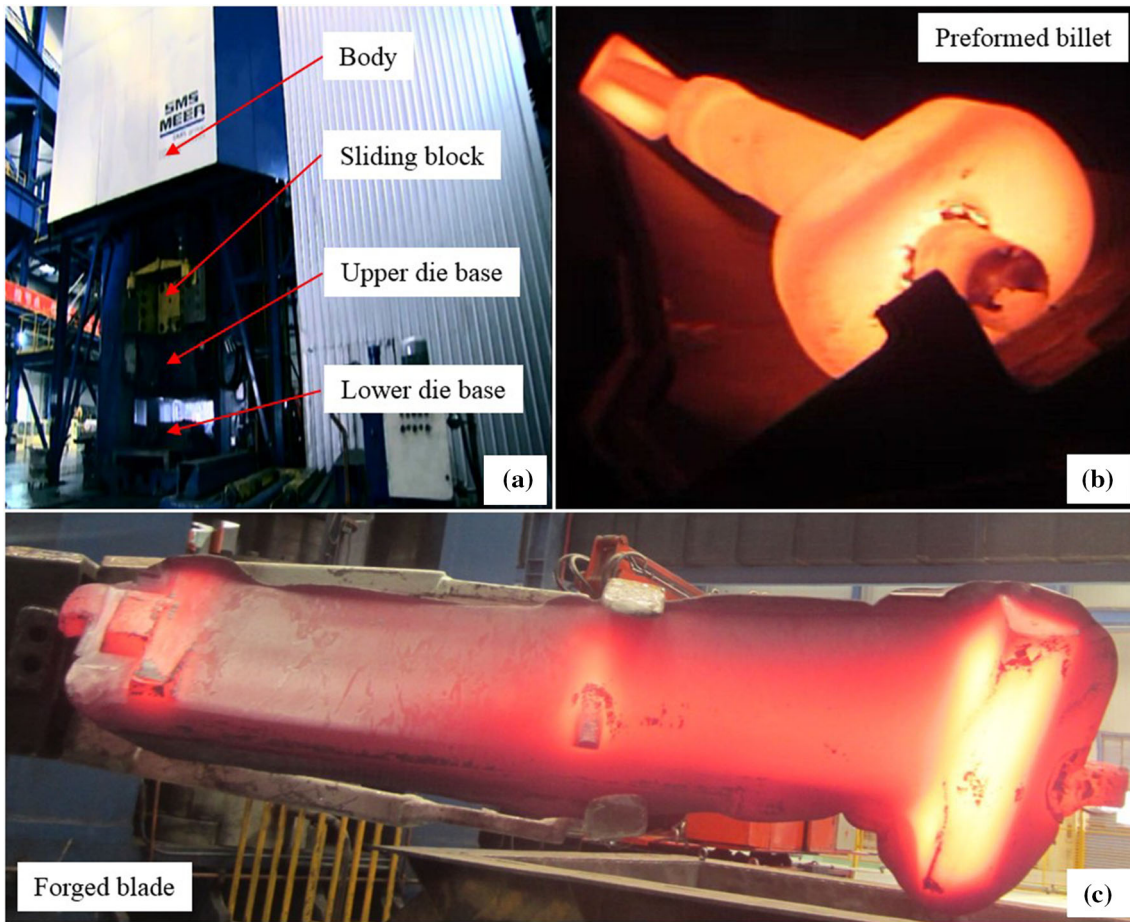


Fig. 3 Experimental setup (a), the preformed billet (b) and forged blade (c)

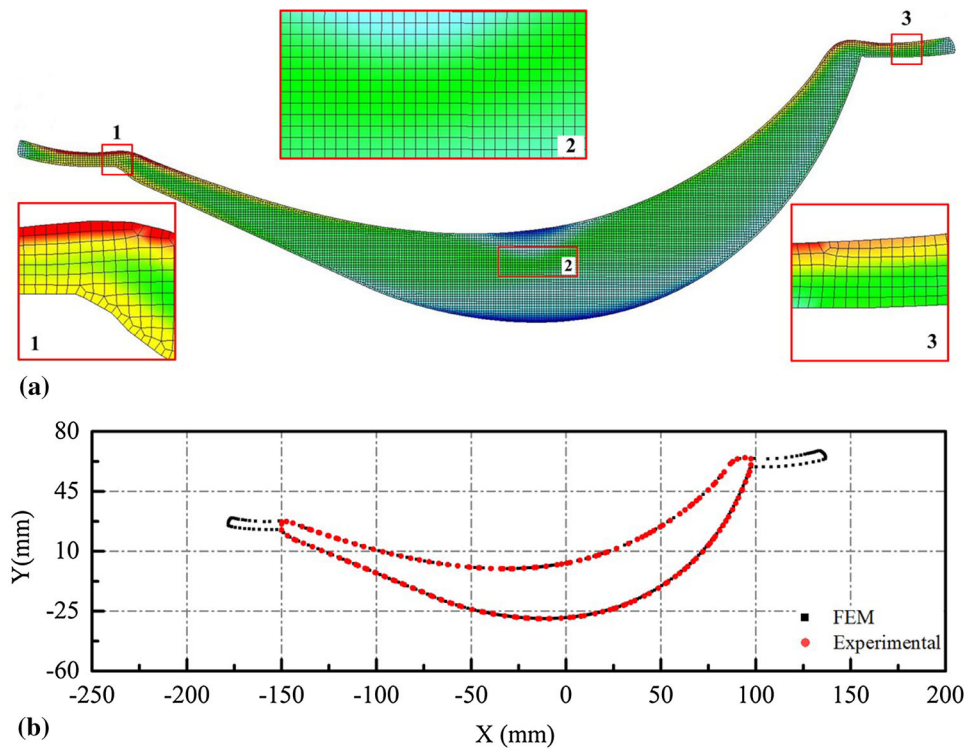


Fig. 4 Mesh details of the forged blade (a) and comparison of the forged blade section with FEM and experimental results (b)

$$D = 2\sqrt{\frac{S_a + S_c}{\pi}} \quad (\text{Eq 10})$$

where  $D$  is the diameter of the preform blade and  $S_a$  and  $S_c$  represent the cross-section areas of the forged blade and flash, respectively.  $S_c$  is often given by Altan et al. (Ref 25)

$$S_c = N_r \times S_a \quad (\text{Eq 11})$$

In Eq 11,  $N_r$  ranges from 5 to 15%, and in this paper, a value of 10% is selected to calculate  $S_c$ . For the given model, the value of  $S_a$  is known as 5828.62 mm<sup>2</sup>; hence,  $D$  is calculated as

$$D = 2\sqrt{\frac{5828.62 + 582.862}{\pi}} = 90.35 \text{ mm} \quad (\text{Eq 12})$$

It is of evidence that friction and its formulation in the numerical simulation greatly influence the accurate prediction of the material deformation. In this paper, the friction at the workpiece-dies interface is assumed to be shear type and expressed as (Ref 26)

$$\tau = mk \quad (\text{Eq 13})$$

where  $\tau$  is the frictional stress,  $m$  is the friction factor and  $k$  is the shear yield stress.

The chemical composition of as-received Ti-6Al-4V is listed in Table 1 (Ref 23).

The temperature-dependent Young's modulus  $E$  (Ref 27), thermal conductivity  $K_a$  (Ref 20) and heat capacity  $C$  (Ref 20) of the blade material can be obtained by Eq 14, 15, and 16, respectively.

$$E = 104.94 - 0.052079 \times T \quad (\text{Eq 14})$$

$$K_a = 0.0131 \times T + 6.45 \quad (\text{Eq 15})$$

$$C = 2.36 + 3 \times 10^{-4} \times T + 2 \times 10^{-6} \times T^2 \quad (\text{Eq 16})$$

where  $T$  denotes the forging temperature of the Ti-6Al-4V blade.

Furthermore, the other important parameters for the FE model are shown in Table 2.

Since the forging process is often accompanied with high temperature and large deformation, the elastic deformation can be negligible and the upper and lower dies are treated as rigid bodies with heat conduction. In addition, the initial position of workpiece and the Quads element type with 10,252 elements

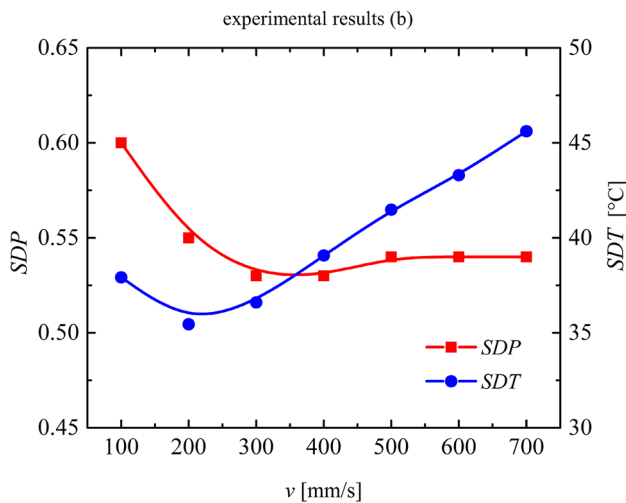


Fig. 5 SDP and SDT variations vs. forging velocity

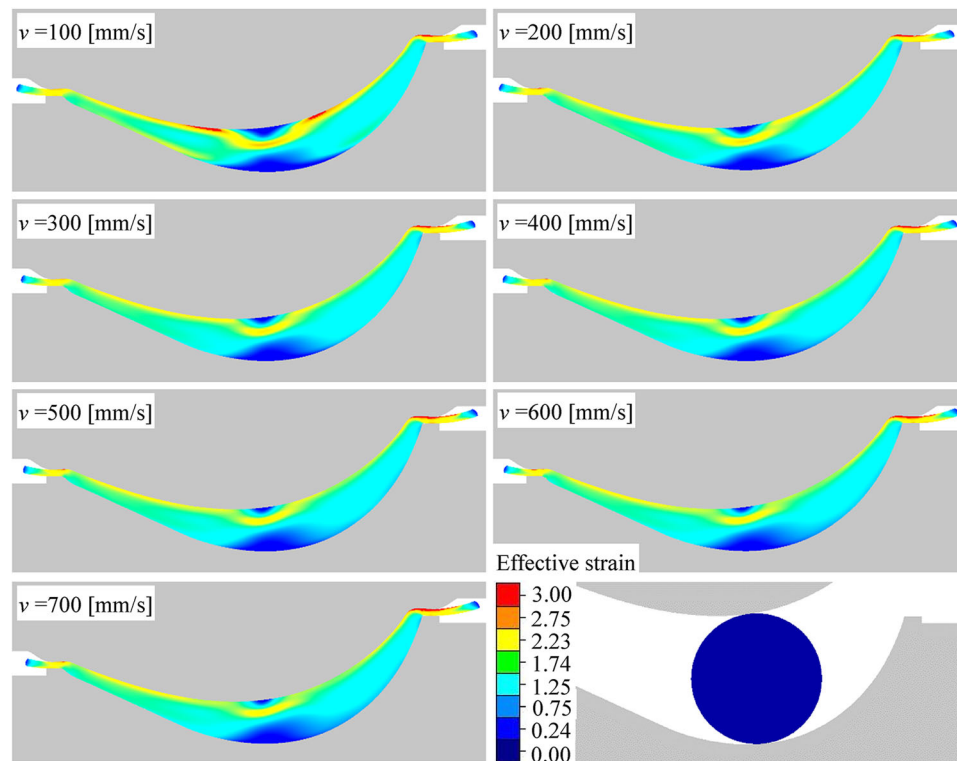


Fig. 6 Distributions of effective strain vs. forging velocity

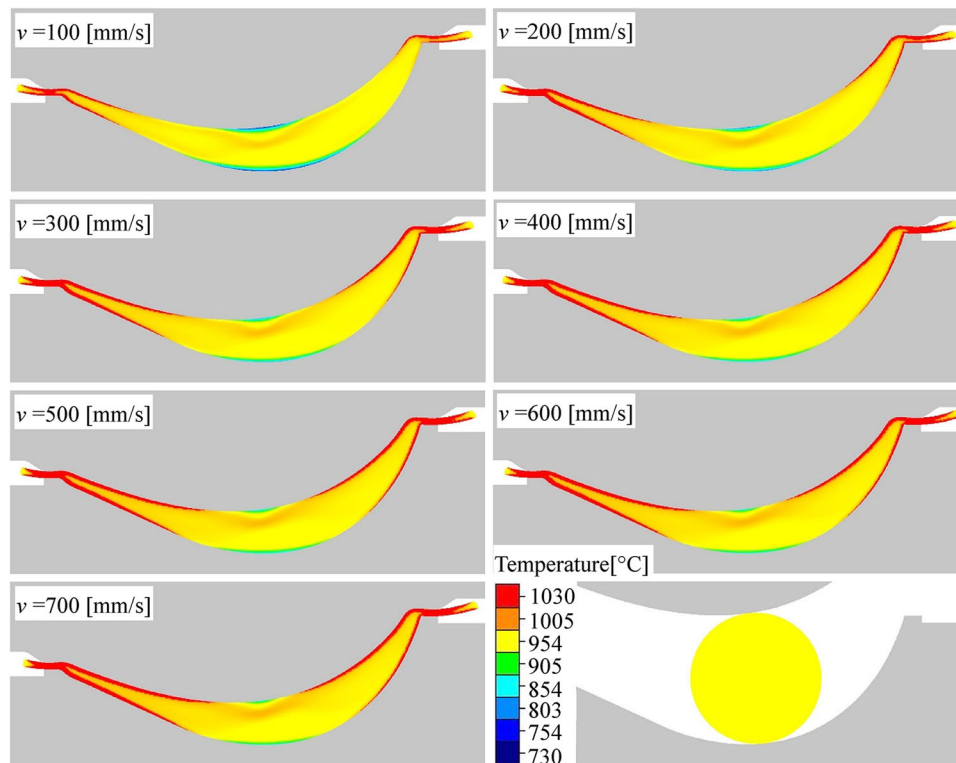


Fig. 7 Distributions of temperature vs. forging velocity

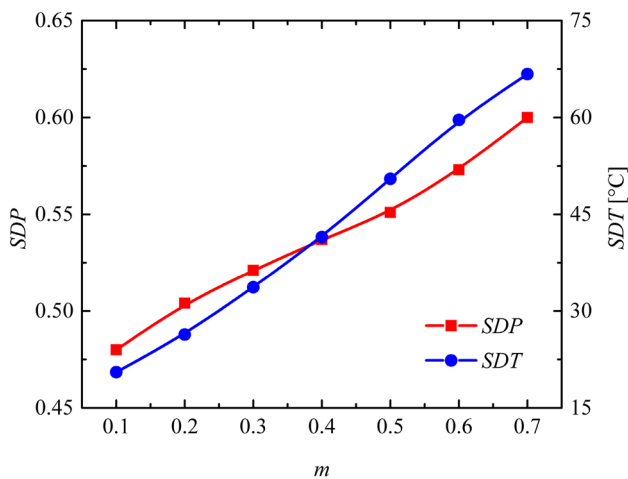


Fig. 8 SDP and SDT variations vs. friction factor

used for the workpiece are shown in Fig. 2. Finally, a 2D remeshing criteria considering the element distortion is employed to solve the severe distortion problem of elements.

### 2.3 Model Validation

The model is run on a HP Z820 workstation with 2.60GHZ Intel Xeon CPU and 32 GB RAM, and about 7 h is utilized to complete the simulation process. As shown in Fig. 3, in order to verify the effectiveness of the FE model, experiments are carried out under the same conditions of simulation on a clutch screw press with the type of SPKA 22400 in Wuxi Turbine Blade Co., Ltd. The parameter DT is set to 30 s considering the

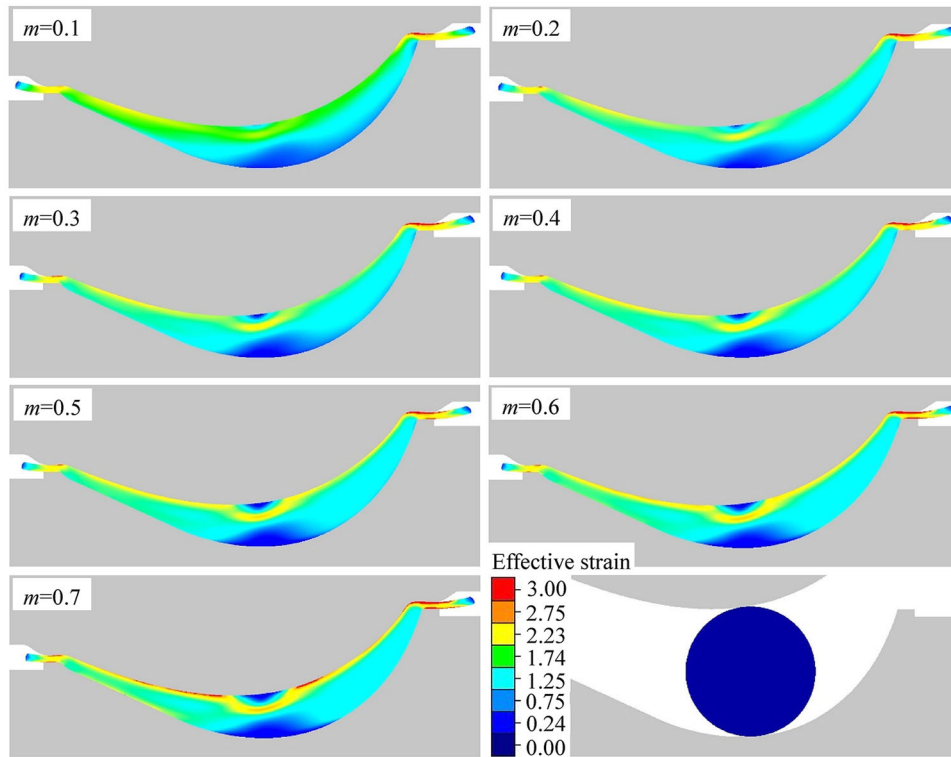
transit time of workpiece. The blade material and other main process parameters are the same as shown in Tables 1 and 2.

Figure 4(a) presents the mesh details of the forged blade, and Fig. 4(b) compares the FEM results of forged blade section with the experimental ones which are measured by a coordinate measuring machine (CMM). Based on the FEM and CMM data, the thickness error on the concave and convex surfaces of the blade section is investigated by the commercial software Geomagic Quality. The average error is found to be only 0.504 mm which is less than 6.3% of the minimum thickness of the forged blade. Moreover, from the work of Hu et al. (Ref 19), the elongation of the blade is small and a reasonable correspondence is found between the 2D and 3D FE analyses in the blade forging operation. Therefore, the 2D FE model is proved to be reliable. The discrepancy between the 2D and 3D FE results may be due to the error resulting from the overconstraint of the metal flow when the forging process is simplified as a plane strain problem.

## 3. Results and Discussion

### 3.1 Simulation Conditions

Employing the established thermo-mechanical FE model, the nonisothermal forging of Ti-6Al-4V turbine blade is thoroughly simulated to investigate the effects of forging velocity  $V$ , friction factor  $m$ , initial workpiece temperature  $T_w$  and dwell time before forging DT on the inside uniformity of deformation and temperature distributions. The simulation conditions characterized by a range of values of  $v = \{100,$



**Fig. 9** Distributions of effective strain vs. friction factor

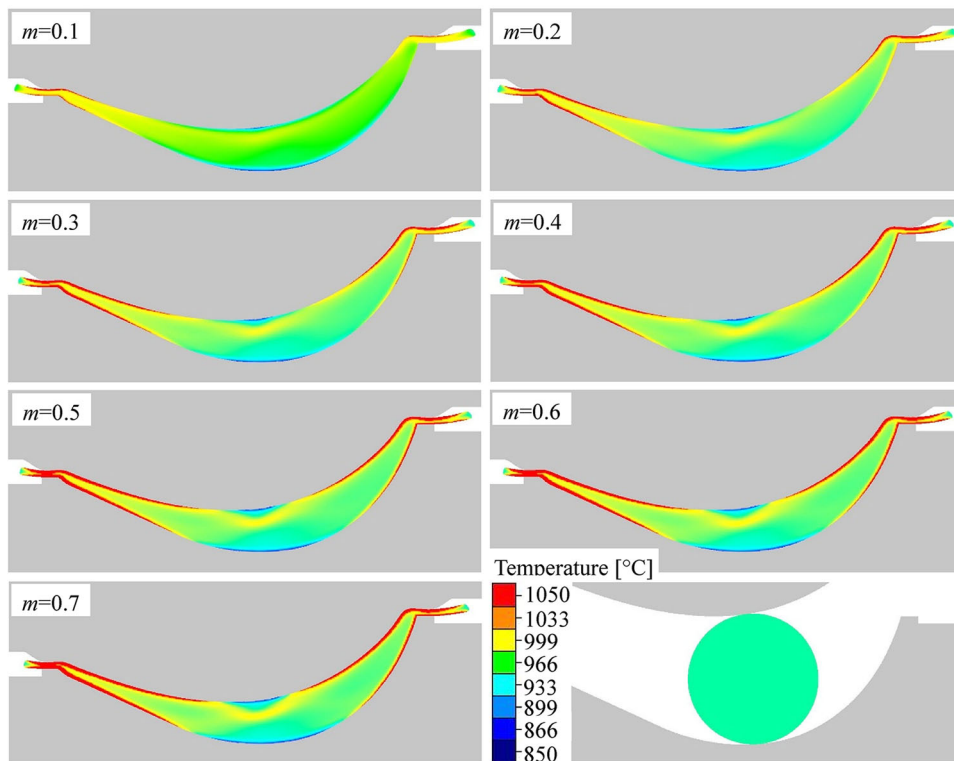


**Fig. 10** Distributions of temperature vs. friction factor

200, 300, 400, 500, 600, 700} (mm/s),  $m = \{0.1, 0.2, 0.3, 0.4, 0.5, 0.6, 0.7\}$ ,  $T_w = \{800, 830, 860, 890, 920, 950, 980\}$  (°C), and  $DT = \{0, 10, 20, 30, 40, 50, 60\}$  (s) are selected, respectively, and the other parameters are kept constant, as shown in Table 2.

### 3.2 Evaluation Indexes

To evaluate the uniformity of strain and temperature distributions in blade forging processes, two indexes are considered. One is the standard deviation of equivalent plastic strain (SDP) which is defined as (Ref 30)

$$SDP = \sqrt{\sum_{i=1}^N (PEEQ_i - PEEQ_a)^2 / (N - 1)} \quad (\text{Eq 17})$$

$$PEEQ_a = \sum_{i=1}^N PEEQ_i / N \quad (\text{Eq 18})$$

where  $PEEQ_a$  is the average of equivalent plastic strain (PEEQ),  $N$  is the number of elements and  $PEEQ_i$  is the PEEQ at element  $i$ . Yang et al. (Ref 3) argued that a smaller SDP value denotes more uniform strain distribution and microstructure.

The other evaluation index is the standard deviation of temperature (SDT) defined as (Ref 30)

$$SDT = \sqrt{\sum_{i=1}^N (T_i - T_a)^2 / (N - 1)} \quad (\text{Eq 19})$$

$$T_a = \sum_{i=1}^N T_i / N \quad (\text{Eq 20})$$

where  $T_a$  is the average temperature and  $T_i$  is the  $T$  at element  $i$ . Like the index of SDP, a smaller SDT value corresponds to more uniform temperature distribution and microstructure.

### 3.3 Effects of Main Process Parameters

**3.3.1 Effects of the Forging Velocity.** Figure 5 shows the variations of SDP and SDT versus the forging velocity. It can be found that, in the defined scope, the SDP becomes not sensitive and tends to stabilize at the level of 0.54 after a sharp decrease when the forging velocity enhances to a medium value of 400 mm/s. This finding indicates that appropriately enhancing the forging velocity of the upper die greatly contributes to

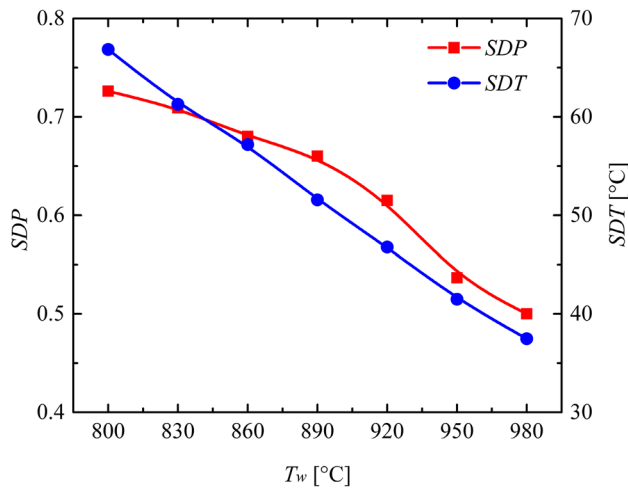


Fig. 11 SDP and SDT variations vs. initial workpiece temperature

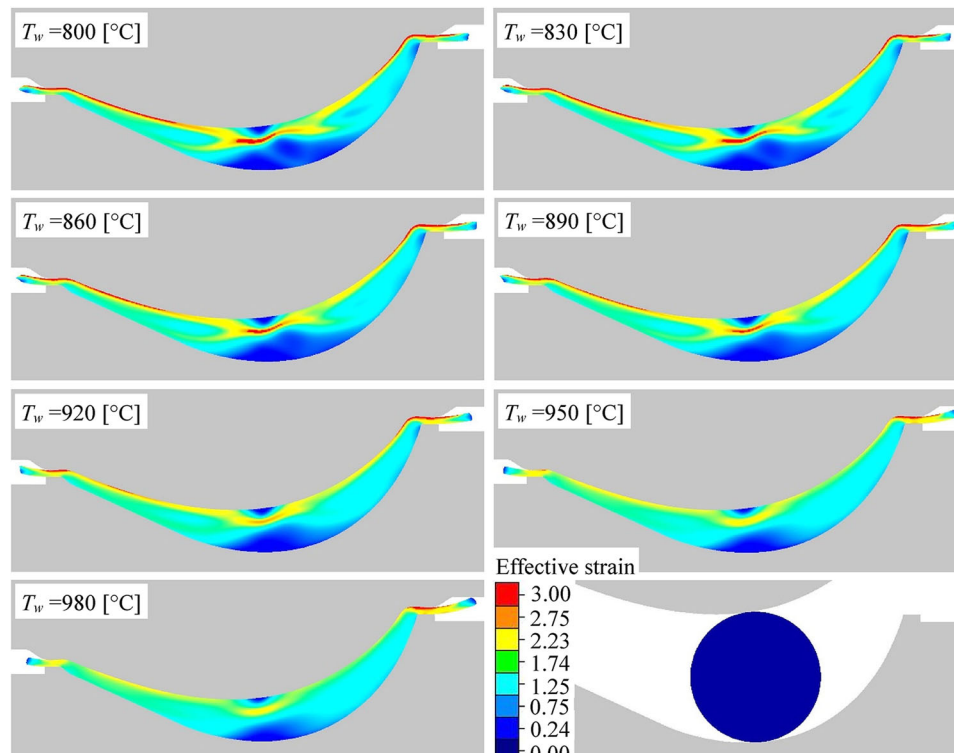


Fig. 12 Distributions of effective strain vs. initial workpiece temperature



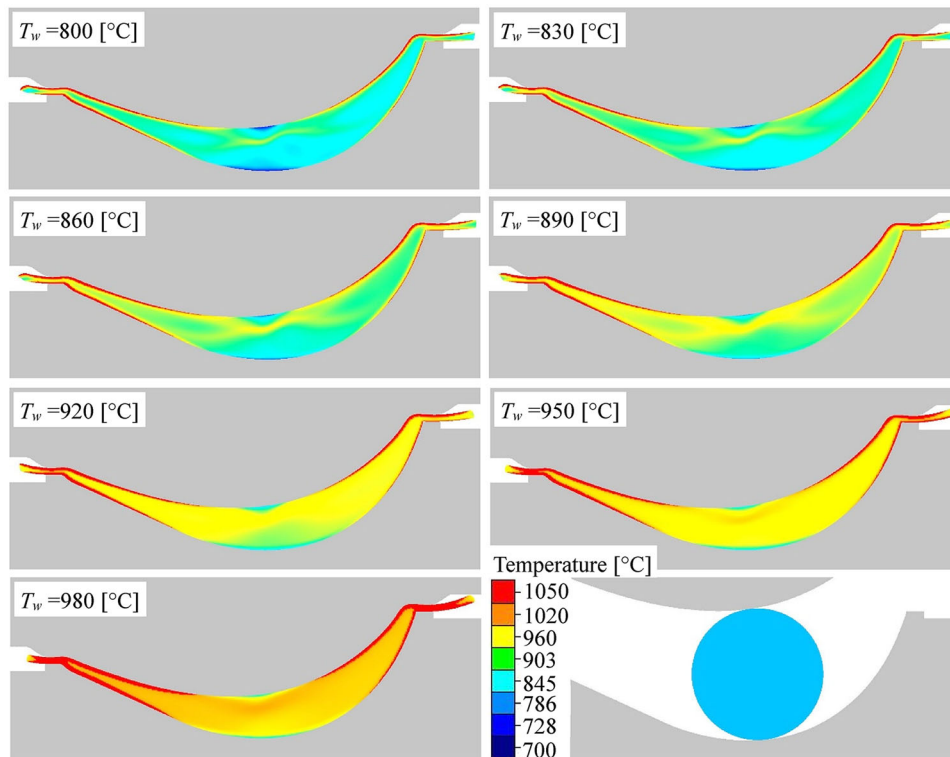


Fig. 13 Distributions of temperature vs. initial workpiece temperature

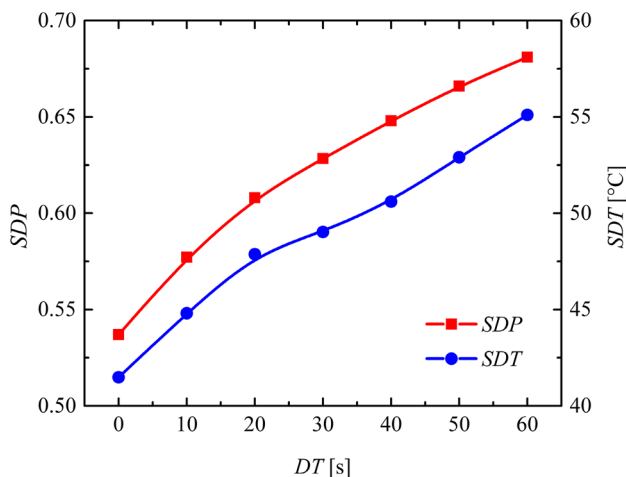
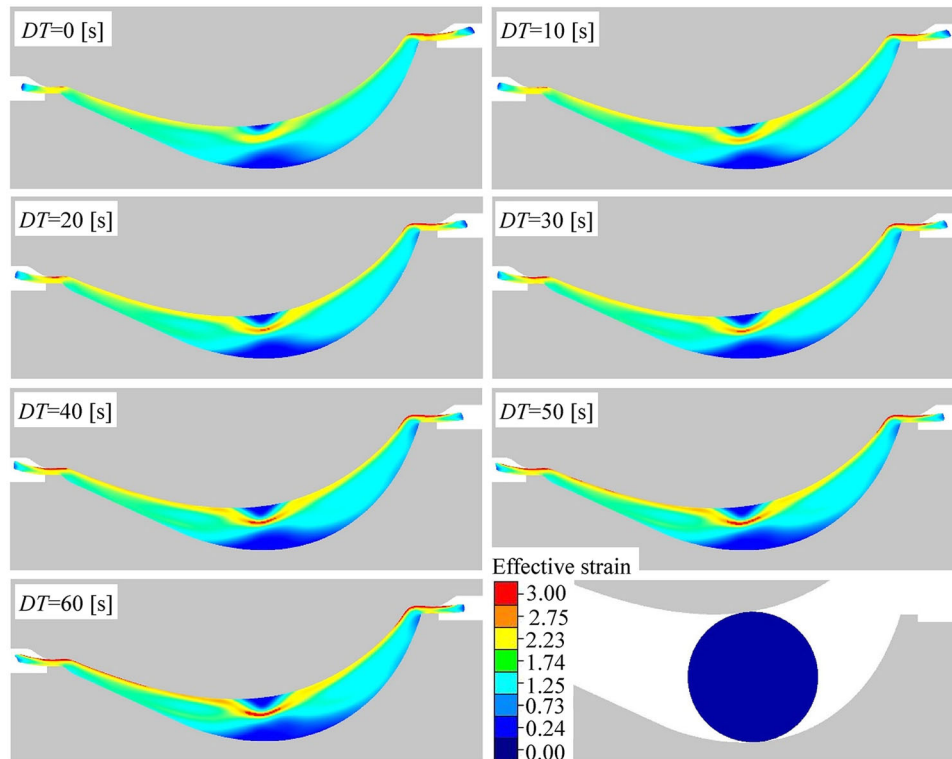


Fig. 14 SDP and SDT variations vs. dwell time

more uniform deformation distribution, as shown in Fig. 6. This is because the larger forging velocity shortens the forming time, leading to less heat loss outside of workpiece in nonisothermal forging process. This view has been supported by Sun et al. (Ref 30) who verified that appropriately enhancing the loading speed can make the deformation more uniform. In contrast, after a slight decrease, the SDT shows a dramatic rise especially when the forging velocity exceeds 300 mm/s. This can be explained by such a fact that larger forging velocity strengthens the deformation and friction heating effects, and this will increase the temperature gap between inside and outside of the workpiece and makes the workpiece temperature distribution less uniform, as shown in Fig. 7.

**3.3.2 Effects of the Friction Factor.** Figure 8 shows the variations of SDP and SDT versus the friction factor. Both the SDP and SDT are observed to show an increasing trend with the increment of the friction factor, corresponding to the tendency of augmented nonuniformity. This indicates that lubrication conditions should be fully considered in the blade forging process to improve the uniformity of deformation and temperature distributions. Furthermore, the inside inhomogeneity of the strain distribution is more evident when the friction factor exceeds 0.3. This finding is in quite agreement with the work by Hu et al. (Ref 10). Specifically, the increased friction factor brings greater flow resistance at the workpiece-dies interface in forging operation; thus, the deformation nonuniformity between the surface layer and the inside of the workpiece becomes more severity, as shown in Fig. 9. This explanation has been fully supported by Yu et al. (Ref 31). For the temperature aspect, the intensive friction increases the heat generation on the workpiece surface caused by the friction heating effect. Moreover, the intensive friction decreases the inside uniformity of the temperature distribution owing to the nonuniformity of the deformation heat distribution generated by the inhomogeneous plastic deformation. The combined effects of these aspects raise the temperature and make the temperature distribution in the forged blade more nonuniform with the enhanced friction factor, as shown in Fig. 10.

**3.3.3 Effects of the Initial Workpiece Temperature.** Figure 11 shows the variations of SDP and SDT versus the initial workpiece temperature. Unlike the friction factor, the initial workpiece temperature shows an opposite influence on the SDP and SDT, and higher temperature values can make the deformation and temperature distributions more uniform. This is because the flow localization of titanium alloys is prone to occur when the deformation is conducted at low temperature, leading to increasing the degree of deformation nonuniformity.



**Fig. 15** Distributions of effective strain vs. dwell time

This view can be directly supported by the investigation of Fan et al. (Ref 32) which reveals the mechanism of flow softening in subtransus hot working of two-phase titanium alloy with equiaxed structure. Moreover, enhancing the initial workpiece temperature decreases the flow stress and further improves the flowability of blade materials. As a consequence, the deformation region expands and the deformation becomes more uniform, as shown in Fig. 12. In addition, by comparing the linear decreasing tendency of SDT in the present work with the finding of linear increasing one in Sun et al. (Ref 30), the lower thermal conductivity of titanium materials and heat transfer coefficient between workpiece and dies are considered to play decisive roles in causing the greater temperature difference than steel materials. On the other hand, the enhanced workpiece temperature improves the plasticity of workpiece and further weakens the thermal effect resulting of deformation; thus, the temperature in the core of the workpiece becomes more uniform. The combined effects of above aspects make the temperature distribution in forging blade more uniform with the increase in initial workpiece temperature, as shown in Fig. 13.

**3.3.4 Effects of the Dwell Time.** Figure 14 shows the variations of SDP and SDT versus the dwell time. Like the friction factor, the dwell time brings the similar trend to the SDP and SDT, and greater dwell time before forging operation makes the deformation and temperature distributions less uniform. This phenomenon is attributed not only to the overall decrease in initial workpiece temperature, but also to the occurrence of deformation temperature gradients which lead to the flow stress gradients and then cause the flow localization of the blade materials. Semiatin and Lahoti (Ref 33) argued that the dwell time is associated with the occurrence of shear bands, and a long value makes the shear bands noticeable. Hence,

decreasing the dwell time can be taken as a means to improve the severity or degree of flow localization, as shown in Fig. 15. On the other hand, due to the long dwell time, the outside temperature of workpiece which cannot be completely compensated by the deformation and friction heating effect is reduced, as shown in Fig. 16, indicating that the dwell time-based analysis of forged uniformity should also fully take the initial workpiece temperature into account.

### 3.4 Overall Evaluation of Process Parameters

Figures 17 and 18 show the overall evaluation of the effects of above four process parameters on the SDP and SDT, respectively. In these charts, each process parameter has been equally weighted, and the points on the overlapping area constituted by the four areas represent the optimal combination of process parameters. A total of seven points, including two from forging velocity, three from friction factors and two from initial workpiece temperature, are observed in Fig. 17, indicating that the optimal combination of process parameters to achieve the deformation uniformity is  $\{v = 400\text{-}500 \text{ mm/s}, m = 0.1\text{-}0.3, T_w = 950\text{-}980 \text{ }^\circ\text{C}\}$ . In contrast, the dwell time has little influence on the optimal solution, and a short dwell time value, however, is expected to further make the strain distribution more uniform. Similarly, it is interesting to observe that the optimal combination of process parameters to achieve the temperature uniformity is the same with the SDP, as shown in Fig. 18. This finding indicates that a reasonable combination of process parameters is indeed existed to achieve the inside deformation and temperature uniformity in the nonisothermal forging of Ti-6Al-4V turbine blades and can provide a significant guidance for the design and optimization of blade forging processes.

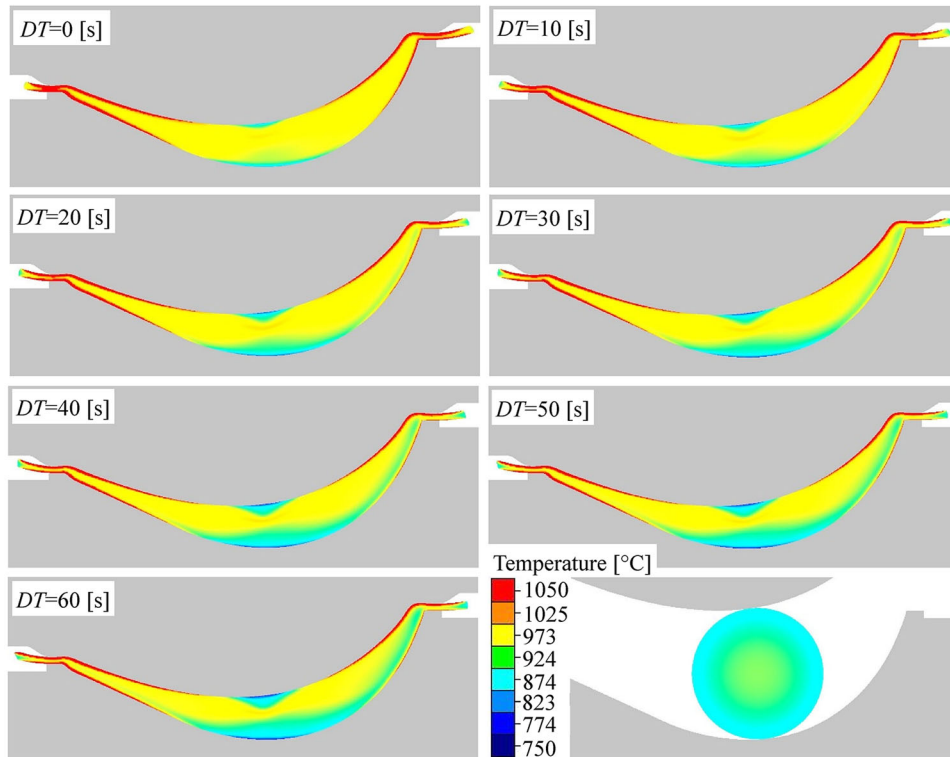


Fig. 16 Distributions of temperature vs. dwell time

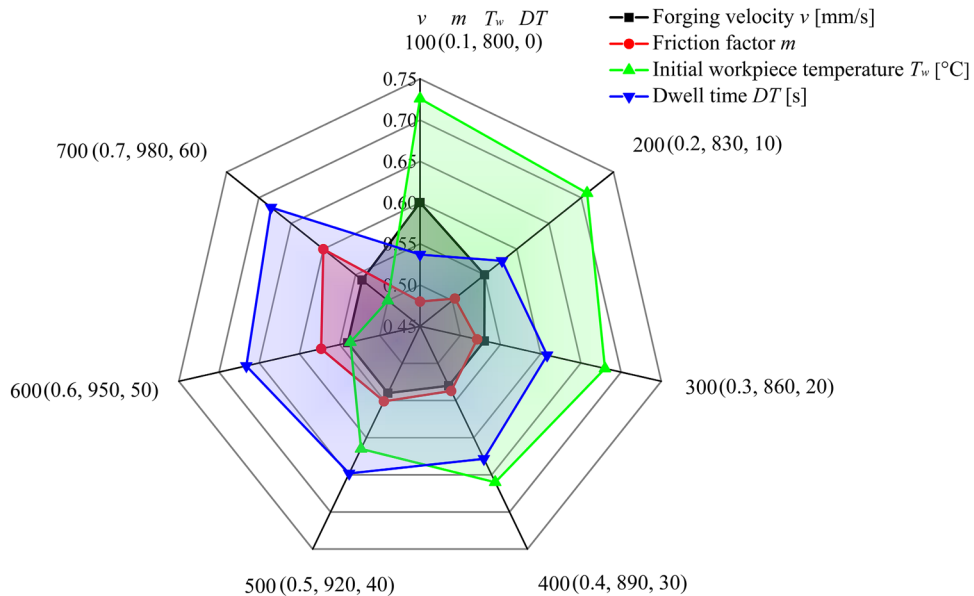
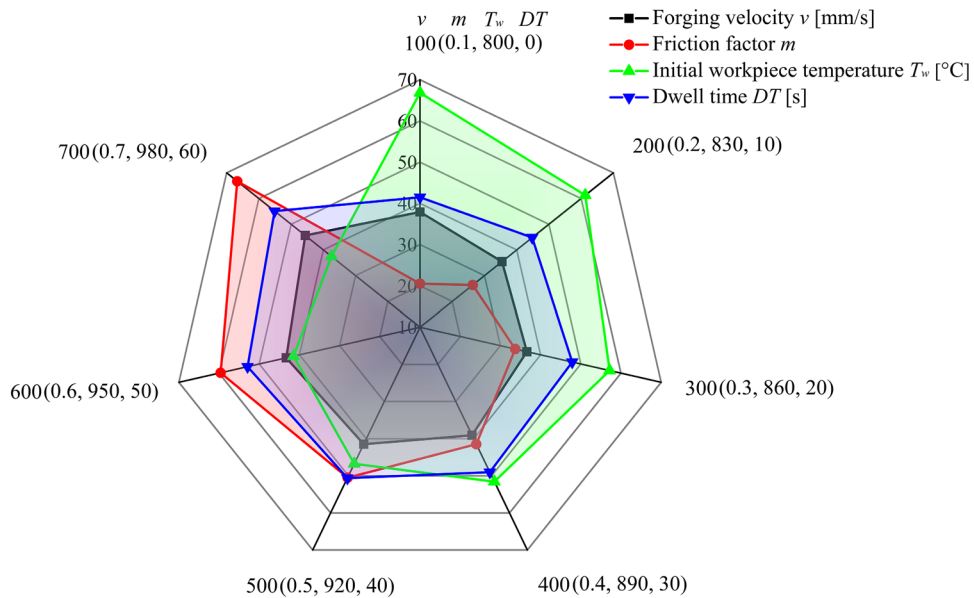


Fig. 17 Overall evaluation of process parameters effects on SDP

#### 4. Application to a Practical Process

After being convinced by the numerical simulation that the determined combination of process parameters serves to promote the forged uniformity without the occurrence of shear bands, glass lubricant-assisted nonisothermal forging experiments under the process parameters  $\{v = 450 \text{ mm/s}, T_w = 960 \text{ }^\circ\text{C}, DT = 8 \text{ s}\}$  are conducted. Figure 19 shows the

macrostructure of one section of the forged blade using the optimized process parameters and microstructures at different locations of the blade section. Uniform macrostructure is observed, and the microstructures at all the locations further demonstrate the stable  $\alpha + \beta$  structures without macro-microdefects such as shear bands and internal crack. Thus, the optimal combination of process parameters determined by numerical simulations is proved to be reasonable and effective.



**Fig. 18** Overall evaluation of process parameters effects on SDT

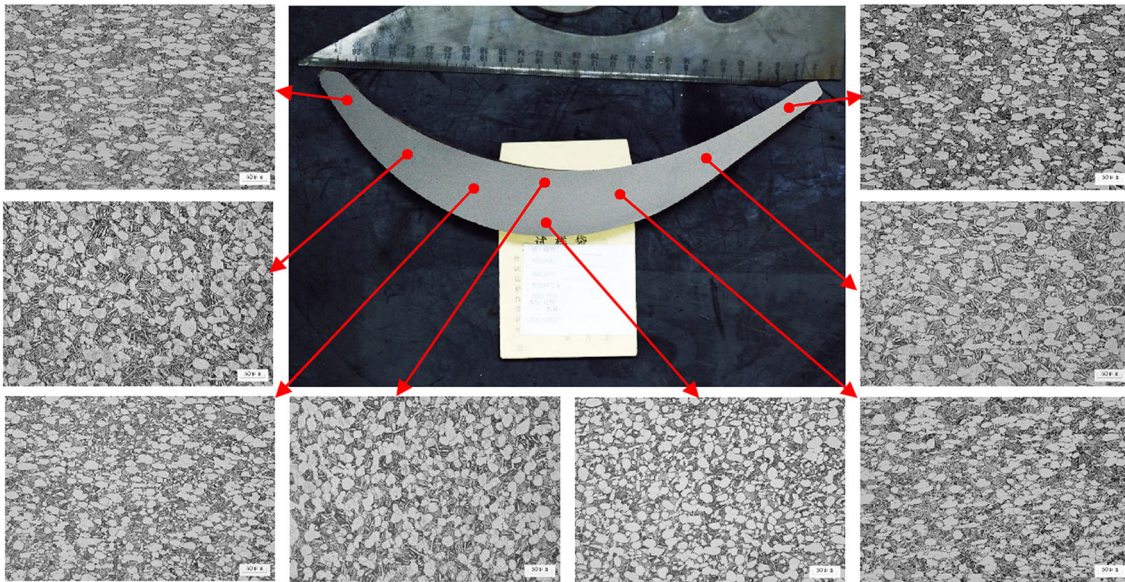


**Fig. 19** Macro- and microstructures of the forged blade section

## 5. Conclusions

Aiming to overcome the nonuniformity in forging processes, macro- and microscale investigation of the forged Ti-6Al-4V blade uniformity is carried out by simulation and experiment in this paper. The influences of four process parameters on the inside deformation and temperature uniformity of the blade are analyzed numerically using the evaluation indexes SDP and SDT and then assessed experimentally. Following conclusions are achieved:

1. The SDP and SDT values are found to be positively correlated with the friction factor and dwell time and negatively correlated with the initial workpiece temperature, indicating that smaller friction factor, shorter dwell time

and higher initial workpiece temperature greatly contribute to the inside deformation and temperature uniformity, respectively. A critical range of forging velocity is existed to obtain the uniform strain and temperature distributions.

2. Essentially, the inside deformation uniformity is attributed to both the lower flow resistance at the workpiece-dies interface and the lower flow softening index at higher deformation temperature. Moreover, the effects of deformation and friction heating are mainly responsible for the temperature uniformity. In addition, a reasonable combination of process parameters  $\{v = 400-500 \text{ mm/s}, m = 0.1-0.3, T_w = 950-980 \text{ °C}\}$  and the least  $DT$  permitted by the production conditions are determined to achieve the uniform strain and temperature distributions.

- The thermo-mechanical FE model showing the dependence of forged uniformity on the four process variables is validated by fitting the experimental and numerical data. In this way, it is possible to implement proper process parameters function directly in the FE numerical code in order to achieve the accurate blade forging simulation with uniformity. This method can also be easily extended to other workpiece materials and forming operations.

## Acknowledgments

The authors would like to gratefully acknowledge the financial support from the National Nature Science Foundation of China (Nos. 51675394, 51375196), the State Key Laboratory of Digital Manufacturing Equipment and Technology (No. DMETKF2016003), the grant from the High-end Talent Leading Program of Hubei Province (No. 2012-86) and the Key R&D Program of Jiangsu Province (No. BE2015005).

## References

- Y.L. Liu, H. Yang, M. Zhan, and Z.X. Fu, A Study of the Influence of the Friction Conditions on the Forging Process of a Blade with a Tenon, *J. Mater. Process. Technol.*, 2002, **123**(1), p 42–46
- S.J. Mirahmadi and M. Hamed, Numerical and Experimental Investigation of Process Parameters in Non-isothermal Forward Extrusion of Ti-6Al-4V, *Int. J. Adv. Manuf. Technol.*, 2014, **75**(1–4), p 33–44
- H. Yang, M. Wang, L.G. Guo, and Z.C. Sun, 3D Coupled Thermo-Mechanical FE Modeling of Blank Size Effects on the Uniformity of Strain and Temperature Distributions During Hot Rolling of Titanium Alloy Large Rings, *Comput. Mater. Sci.*, 2008, **44**(2), p 611–621
- L.E. Murr, A.C. Ramirez, S.M. Gaytan, M.I. Lopez, E.Y. Martinez, D.H. Hernandez, and E. Martinez, Microstructure Evolution Associated with Adiabatic Shear Bands and Shear Band Failure in Ballistic Plug Formation in Ti-6Al-4V Targets, *Mater. Sci. Eng., A*, 2009, **516**(1), p 205–216
- E. Alabort, D. Putman, and R.C. Reed, Superplasticity in Ti-6Al-4V: Characterisation, Modelling and Applications, *Acta Mater.*, 2015, **95**, p 428–442
- F. Cao, P. Kumar, M. Koopman, C. Lin, Z.Z. Fang, and K.R. Chandran, Understanding Competing Fatigue Mechanisms in Powder Metallurgy Ti-6Al-4V Alloy: Role of Crack Initiation and Duality of Fatigue Response, *Mater. Sci. Eng., A*, 2015, **630**, p 139–145
- N.K. Park, J.T. Yeom, and Y.S. Na, Characterization of Deformation Stability in Hot Forging of Conventional Ti-6Al-4V Using Processing Maps, *J. Mater. Process. Technol.*, 2002, **130**, p 540–550
- G. Zhou, L. Hua, D.S. Qian, D.F. Shi, and H.X. Li, Effects of Axial Rolls Motions on Radial-Axial Rolling Process for Large-Scale Alloy Steel Ring with 3D Coupled Thermo-Mechanical FEA, *Int. J. Mech. Sci.*, 2012, **59**(1), p 1–7
- F. Chen, F.C. Ren, J. Chen, Z.S. Cui, and H.G. Ou, Microstructural Modeling and Numerical Simulation of Multi-physical Fields for Martensitic Stainless Steel During Hot Forging Process of Turbine Blade, *Int. J. Adv. Manuf. Technol.*, 2015, doi: [10.1007/s00170-015-7368-8](https://doi.org/10.1007/s00170-015-7368-8)
- C.L. Hu, H.G. Ou, and Z. Zhao, An Alternative Evaluation Method for Friction Condition in Cold Forging by Ring with Boss Compression Test, *J. Mater. Process. Technol.*, 2015, **224**, p 18–25
- J.C. Wang, L. Langlois, M. Rafiq, R. Bigot, and H. Lu, Study of the Hot Forging of Weld Cladded Work Pieces Using Upsetting Tests, *J. Mater. Process. Technol.*, 2014, **214**, p 365–379
- B.S. Kang, N. Kim, and S. Kobayashi, Computer-Aided Preform Design in Forging of an Airfoil Section Blade, *Int. J. Mach. Tools Manuf.*, 1990, **30**(1), p 43–52
- H. Ou and R. Balendra, Preform Design for Forging of Aerofoil Sections Using FE Simulation, *J. Mater. Process. Technol.*, 1998, **80**, p 144–148
- M. Zhan, Y.L. Liu, and H. Yang, Influence of the Shape and Position of the Preform in the Precision Forging of a Compressor Blade, *J. Mater. Process. Technol.*, 2002, **120**, p 80–83
- H. Ou, C.G. Armstrong, and M.A. Price, Die Shape Optimisation in Forging of Aerofoil Sections, *J. Mater. Process. Technol.*, 2003, **132**(1), p 21–27
- B. Lu, H. Ou, C.G. Armstrong, and A. Rennie, 3D Die Shape Optimisation for Net-Shape Forging of Aerofoil Blades, *Mater. Des.*, 2009, **30**(7), p 2490–2500
- A. Kocańda, P. Czyżewski, and K.H. Mehdi, Numerical Analysis of Lateral Forces in a Die for Turbine Blade Forging, *Arch. Civ. Mech. Eng.*, 2009, **9**(4), p 49–54
- S.Y. Luo, D.H. Zhu, D.S. Qian, L. Hua, S.J. Yan, and J.J. Zhang, Effects of Friction Model on Forging Process of Ti-6Al-4V Turbine Blade Considering the Influence of Sliding Velocity, *Int. J. Adv. Manuf. Technol.*, 2015, doi: [10.1007/s00170-015-7538-8](https://doi.org/10.1007/s00170-015-7538-8)
- Z.M. Hu, J.W. Brooks, and T.A. Dean, Three-Dimensional Finite Element Modelling of Forging of a Titanium Alloy Aerofoil Sectioned Blade, *J. Manuf. Sci. Eng.*, 1999, **121**(3), p 366–371
- V. Alimirzaloo, M.H. Sadeghi, and F.R. Biglari, Optimization of the Forging of Aerofoil Blade Using the Finite Element Method and Fuzzy-Pareto Based Genetic Algorithm, *J. Mech. Sci. Technol.*, 2012, **26**(6), p 1801–1810
- Y. Shao, B. Lu, H. Ou, and J. Chen, A New Approach of Preform Design for Forging of 3D Blade Based on Evolutionary Structural Optimization, *Struct. Multidiscip. Optim.*, 2014, **51**(1), p 199–211
- S.H.R. Torabi, S. Alibabaei, B.B. Bonab, M.H. Sadeghi, and G. Faraji, Design and Optimization of Turbine Blade Preform Forging Using RSM and NSGA II, *J. Intell. Manuf.*, 2015, doi: [10.1007/s10845-015-1058-0](https://doi.org/10.1007/s10845-015-1058-0)
- J. Cai, K.S. Wang, P. Zhai, F.G. Li, and J. Yang, A Modified Johnson-Cook Constitutive Equation to Predict Hot Deformation Behavior of Ti-6Al-4V Alloy, *J. Mater. Eng. Perform.*, 2015, **24**(1), p 32–44
- J. Cai, F.G. Li, T.Y. Li, B. Chen, and M. He, Constitutive Equations for Elevated Temperature Flow Stress of Ti-6Al-4V Alloy Considering the Effect of Strain, *Mater. Des.*, 2011, **32**(3), p 1144–1151
- T. Altan, G. Ngaile, and G. Shen, *Cold and Hot Forging: Fundamentals and Applications*, ASM International, Materials Park, 2004
- C. Lv, L. Zhang, Z.J. Mu, Q.G. Tai, and Q.Y. Zheng, 3D FEM Simulation of the Multi-stage Forging Process of a Gas Turbine Compressor Blade, *J. Mater. Process. Technol.*, 2008, **198**(1), p 463–470
- K.T. Kim and H.C. Yang, Densification Behavior of Titanium Alloy Powder During Hot Pressing, *Mater. Sci. Eng., A*, 2001, **313**(1), p 46–52
- Y.C. Zhu, W.D. Zeng, X. Ma, Q.G. Tai, Z.H. Li, and X.G. Li, Determination of the Friction Factor of Ti-6Al-4V Titanium Alloy in Hot Forging by Means of Ring-Compression Test Using FEM, *Tribol. Int.*, 2011, **44**(12), p 2074–2080
- R.S. Lee and H.C. Lin, Process Design Based on the Deformation Mechanism for the Non-isothermal Forging of Ti-6Al-4V Alloy, *J. Mech. Sci. Technol.*, 1998, **79**(1), p 224–235
- Z.C. Sun, H. Yang, and X.F. Guo, FE Analysis on Deformation and Temperature Nonuniformity in Forming of AISI-5140 Triple Valve by Multi-way Loading, *J. Mater. Eng. Perform.*, 2013, **22**(2), p 358–365
- H.Q. Yu and J.D. Chen, *Principles of Metal Forming*, China Machine Press, Beijing, 1999 (in Chinese)
- X.G. Fan, H. Yang, and P.F. Gao, The Mechanism of Flow Softening in Subtransus Hot Working of Two-Phase Titanium Alloy with Equiaxed Structure, *Chin. Sci. Bull.*, 2014, **59**(23), p 2859–2867
- S.L. Semiatin and G.D. Lahoti, The Occurrence of Shear Bands in Nonisothermal, Hot Forging of Ti-6Al-2Sn-4Zr-2Mo-0.1Si, *Mater. Trans. A*, 1983, **14**(1), p 105–115